ARTICLE
Journal of Cellular Biochemistry 113:1397–1406 (2012)

Journal of Cellular Biochemistry

Intratumoral Injection of Taxol In Vivo Suppresses A549 Tumor Showing Cytoplasmic Vacuolization

Chaoyang Wang and Tongsheng Chen*

MOE Key Laboratory of Laser Life Science & Institute of Laser Life Science, College of Biophotonics, South China Normal University, Guangzhou 510631, China

ABSTRACT

Based on our recent in vitro studies, this report was designed to explore the mechanism by which high concentration of taxol (70 μM) induced paraptosis-like cell death in human lung carcinoma (A549) cells, and to evaluate the therapeutic efficacy of taxol using A549 tumor-bearing mice in vivo. Exposure of cells to taxol induced time-dependent cytotoxicity and cytoplasmic vacuolization without the involvement of Bax, Bak, Mcl-1, Bcl-XL, and caspase-3. Although taxol treatment induced activating transcription factor 6 (ATF6) cleavage indicative of endoplasmic reticulum (ER) stress, silencing ATF6 by shATF6 did not prevent taxol-induced both cytotoxcity and cytoplasmic vacuolization, suggesting that taxol-induced cytoplasmic vacuolization and cell death were not due to ER stress. Moreover, taxol-treated cells did not show DNA fragmentation and loss of mitochondrial membrane potential, the typical characteristics of apoptosis. In addition, taxol-induced cytoplasmic vacuolization did not show the cellular lysis, the characteristics of oncosis, and positive of β-galactosidase, the characteristic of senescence, indicating that taxol induced paraptosis-like cell death is neither oncosis nor senescence. Moreover, our in vivo data showed that intratumoral injection of taxol (50 mg/kg) in A549 tumor xenograft mice on day 1 and day 19 potently suppressed tumor growth showing significant ER vacuolization without toxicity. In conclusion, high concentration of taxol exhibits a significant anticancer activity by inducing paraptosis-like cell death in vitro and in vivo, without significant toxicity, suggesting a promising therapeutic strategy for apoptosis-resistance cancer by inducing ER vacuolization. J. Cell. Biochem. 113: 1397–1406, 2012.

KEY WORDS: TAXOL; A549 CELLS; CYTOPLASMIC VACUOLIZATION; ENDOPLASMIC RETICULUM (ER); PARAPTOSIS-LIKE CELL DEATH; APOPTOSIS; SENESCENCE; ONCONSIS; INTRATUMORAL INJECTION

Taxol resistance challenged all specialists, although taxol has been used in the treatment of broad range of tumor types, including non-small cell lung cancer (NSCLC), breast and ovarian cancers [Fields and Runowicz, 2003; Crown et al., 2004]. The hydrophobic nature of taxol can induce overexpression of the multidrug resistance 1 (MDR1) gene [Horwitz et al., 1993]. Cells expressing high levels of the multidrug resistance (MDR)–associated protein MRP displayed no or low resistance to taxol [Zaman et al., 1994]. Monzó et al. demonstrated that beta-tubulin gene mutations as a strong predictor of response to the antitubulin drug taxol [Monzó et al., 1999]. Ishibashi et al. showed that overexpression of NAC-1, a transcriptional repressor, was essential for taxol resistance and tumor recurrence [Ishibashi et al., 2008]. However, the mechanism under taxol resistance is still unclear.

Taxol mainly induces apoptosis in tumor cells and taxol resistance results from activation of Akt pathway and/or disorder of apoptosis pathway facilitating survival of cells [Szanto et al., 2009]. The type of taxol-induced cell death is concentration-dependent [Torres and Horwitz, 1998]. Some reports showed that taxol induces apoptosis in lower concentration range (5–50 nM) and necrosis in higher concentration range (0.1–50 μM) [Yeung et al., 1999; Mailloux et al., 2001; Pushkarev et al., 2008; Li et al., 2009; Stepien et al., 2010; Yu et al., 2011]. Recently, we for the first time reported that taxol (70 μM) induced paraptosis-like cell death

Abbreviations: ATF6, activating transcription factor 6; CCK-8, Cell Counting Kit-8; DQMD, D(OMe)QMD(OMe); DTT, dithiothreitol; EGFP, enhanced green fluorescence protein; ER, endoplasmic reticulum; FCM, flow cytometry; HE, hematoxylin and eosin; NSCLC, non-small cell lung cancer; Rho 123, rhodamine 123; SA-β-gal, senescence-associated beta-galactosidase; shRNA, short hairpin RNA; STS, staurosporine; $\Delta\Psi_m$, mitochondrial membrane potential.

Grant sponsor: National Natural Science Foundation of China; Grant numbers: 31071218, 61178078.

*Correspondence to: Prof. Tongsheng Chen, PhD, Institute of Laser Life Science, South China Normal University, Guangzhou 510631, China. E-mail: chentsh@scnu.edu.cn

Received 22 November 2011; Accepted 23 November 2011 • DOI 10.1002/jcb.24012 • © 2011 Wiley Periodicals, Inc.
Published online 1 December 2011 in Wiley Online Library (wileyonlinelibrary.com).

showing caspase independency and cytoplasmic vacuolization largely due to endoplasmic reticulum (ER) swelling [Chen et al., 2008; Sun et al., 2010], suggesting that ER plays an important role in taxol-induced cell death, and may be a new target of taxol-based chemotherapy for apoptosis-resistance cancer.

Cytoplasmic vacuolization is also the morphologic characteristic of both oncosis and senescence [Majno and Joris, 1995; Chang et al., 1999]. Senescence, a physiological process that limits the proliferative span of normal cells, is accompanied by morphological changes (enlarged and flattened shape and increased granularity), shortening of telomeres, and accumulation of karyotypic abnormalities [Hayflick and Moorhead, 1961; Smith and Pereira-Smith, 1996; Duncan and Reddel, 1997]. In addition, a commonly used surrogate marker of senescence in human cells is the SA-β-gal active at pH 6.0 [Dimri et al., 1995]. Moreover, oncosis is characterized by plasma membrane blebbing, dilation of the ER, mitochondrial swelling, and clumping of the nuclear chromatin [Majno and Joris, 1995]. These morphological changes are followed by the breakdown of the plasma membrane, release of intracellular constituents, and inflammation. Whether taxol-induced cell death showing cytoplasmic vacuolization is in senescence or oncosis is unclear.

Recently, taxol has become the appropriate candidate by intratumoral injection against breast, prostate, and bladder tumors and suppressed the tumor with little toxic side effects [Shikanov et al., 2008; Al-Ghananeem et al., 2009; Shikanov et al., 2009]. The potential of taxol attracts attention to new adjuvant treatment by direct intratumoral injection against NSCLC which accounts for 80% of all lung cancer patients and is the leading cause of cancer-related death in both men and women all over the world [Celikoglu et al., 2008; Pallis et al., 2009], although the reports concerning this field are not universally demonstrated. The potential advantages for direct intratumoral drug injection include (i) assured precision in the local delivery of drugs, (ii) complete perfusion of drug within and around the lesion, (iii) dramatically higher tumor tissue concentrations than is achievable by conventional systemic chemotherapy, and (iv) little or no systemic toxic side effects [Celikoglu et al., 2008].

The objective of this study is to further explore the molecular mechanism and the form of taxol-induced cell death showing cytoplasmic vacuolization in vitro in human lung adenocarcinoma (A549) cells, and to evaluate the in vivo effect of intratumoral injection of taxol on suppressing tumor growth using A549 tumor xenograft model. Our in vitro study firstly identified that Bax, Bak, Mcl-1, Bcl-XL, ER stress, and mitochondria did not participate in the taxol-induced paraptosis-like cell death that is neither senescence nor oncosis. Furthermore, our in vivo data showed that intratumoral injection of taxol potently suppressed tumor growth showing obvious ER vacuolization.

MATERIALS AND METHODS

REAGENTS

Taxol was purchased from Haikou Pharmaceutical Co. (Haikou, China). Hoechst 33258 was obtained from Sigma (St. Louis, MO). Cell Counting Kit (CCK-8) was purchased from Dojindo Laboratories (Kumamoto, Japan). Staurosporine (STS) was purchased from Alexis (Lausen, Switzerland). Ethyl 2-amino-6-bromo-4- (1-cyano-2-ethoxy-2-oxoethyl)-4H-chromene-3-carboxylate (HA14-1) was purchased from Alexis Biochemicals (Lausen, Switzerland). Senescence β-Galactosidase Staining Kit (Genmed Scientifics Inc., Wilmington, NC). Rabbit polyclonal ATF6 antibody and mouse polyclonal β-actin antibody were obtained from Santa Cruz Biotechnology (Santa Cruz, CA).

CELL CULTURE AND TRANSFECTION

A549 cell line obtained from the Department of Medicine, Jinan University (Guangzhou, China), was cultured in Dulbecco's modified Eagle's medium (DMEM, Gibco, Grand Island, NY) supplemented with 10% fetal calf serum. Cell cultures were maintained at 37°C in a humidified 5% CO_2 incubator. Plasmids DNA of EGFP were transiently transfected into the cells by using Lipofectamine 2000 (Invitrogen, Carlsbad, CA).

shRNA AND TRANSFECTION

For silencing experiments, A549 cells were seeded at 1×10^5 cells per well in 24-well plates and allowed to reach ~50% confluence on the day of transfection. Cells were transiently transfected with 0.5–0.8 μg Bak shRNA, Bax shRNA, Mcl-1 shRNA, ATF6 shRNA, or negative control shNC (GenePharma, Shanghai, China), respectively, using Turbofect^{TM} siRNA transfection reagent (Fermentas International Inc, Burlington, ON, Canada) according to the manufacturer's transfection protocol. Twenty-four hours after transfection, cells were split into 96-well plates at a density of 8×10^3 for detection of cell viability. Efficiency of shRNA was measured by Western blotting analysis. The oligonucleotides for shRNA were synthesized as follows: shBax: 5′-GGGACGAACTGGACAGTAACATTCAAGA-GATGTTACTGTCCAGTTCGTC- CCTT-3′; shBak: 5′-GCCTGTTTGA-GAGTGGCATCATTCAAGAGATGATGCCACTCTCAAAC- AGGCTT-3′; shMcl-1: 5′-GGUUUGGCAUAUCUAAUAA-3′; shATF6: 5′-TGCTG-TTGACAGTG-AGCGCGGAGACAGCAACGTATGATAATA-GTGAAG-CACAGATGTATTATCATACGTTGC-TGTCTCCTTGCCTACTGCCT-CGGA-3′; shNC: 5′-GTTCTCCGAACGTGTCACGTCAAGAGAT-TACGTGA-CACGTTCGG-AGAA-TT-3′.

MEASUREMENT OF MITOCHONDRIAL MEMBRANE POTENTIAL (ΔΨM)

Rhodamine 123 (Rho 123, Sigma) was used to analyze ΔΨm by flow cytometric (FCM) assay as previously described [Lu et al., 2010]. Briefly, cells were harvested and stained with 10 μM Rho 123 for 30 min at 37°C in the dark, and then washed with PBS twice and subsequently assayed by FCM. Results were expressed as the proportion of cells with low Rho123 fluorescence indicating the loss of ΔΨm.

ASSAY OF CELL VIABILITY AND HOECHST 33258 STAINING

Cell viability was assessed by Cell Counting Kit-8 (CCK-8, Dojindo) assay as described previously [Sun et al., 2010]. All experiments were performed in quadruple occasions. Cells were grown on the coverslip of a 35-mm chamber. After being washed with PBS three times, cells were stained with 1 μM Hoechst 33258 20 min at room temperature. The cells were then washed three times with PBS and the images were recorded using a digital camera (Nikon, Tokyo, Japan) with 1,280 × 1,280 pixels resolution.

MONITORING OF CYTOPLASMIC VACUOLIZATION AND THE ROLE OF Bcl-XL INSIDE LIVING CELLS

Cytoplasmic vacuolization was observed using confocal fluorescence microscopy (LSM510, Zeiss, Jena, Germany). Cells expressing EGFP were treated with or without 70 μM taxol for 24 h. For assay of participation of Bcl-XL, HA14-1 was added to the medium 1 h before treatment with taxol for 18 h. All the quantitative analysis of the fluorescence images was performed by Zeiss Rel 3.2 image processing software (Zeiss). EGFP was excited at 488 nm and fluorescence emission was recorded through a 500–550 nm band-pass filter.

WESTERN BLOTTING ANALYSIS

Cells were lysed in lysis buffer (50 mM Tris-HCl, pH 8.0, 150 mM NaCl, 1% Triton-100, 1 mM PMSF, and protease inhibitor cocktail set I. After removing insoluble material by centrifugation for 5 min at 12,000 × *g*, the protein concentration was estimated in the supernatant using the Bio-Rad protein assay (Bio-Rad, Munich, Germany) according to the manufacturer's protocol. Protein was separated by SDS-PAGE under reducing conditions before transferring onto nitrocellulose membranes (Millipore, Billerica, MA). Blots were blocked in TBST buffer containing 5% non-fat dry milk for 1 h at room temperature. The membrane was incubated overnight at 4°C with the respective primary antibodies. After repeated washings with TBST, the membranes were incubated with the secondary antibody for 1 h at room temperature before continuing to wash with TBST. Detection was performed using the Odyssey Infrared Imaging System (LI-COR Biosciences, Nebraska). Equal loading was verified by antibody against β-Actin.

SENESCENCE ASSAY

Cells of 10^6 cells/mL were seeded into 24 wells plate. Twenty-four hours later, taxol and H_2O_2 (300 μM) were added to the medium for 24 h respectively, then cells were stained by Senescence β-Galactosidase Staining Kit, according to the supplier recommendations. Cells were washed twice with PBS, fixed for 5 min in 2% formaldehyde/0.2% glutaraldehyde, washed again with PBS, and then incubated for 16 h at 37°C(no CO_2) in fresh senescence-associated β-galactosidase (SAβ-gal) buffer [1 mg/mL X-Gal, 5 mmol/L potassium ferrocyanide, 5 mmol/L potassium ferricyanide, 2 mmol/L $MgCl_2$ in PBS (pH 6.0)]. SAβ-gal activity results in a blue staining that can be visualized by light microscopy.

TUMOR INOCULATION AND TREATMENT

All animal experimentation described in this study was performed in accordance with and approved by the institutional animal care and use committee. Female 6–8-week-old athymic nude mice (BALB/c strain) purchased from Southern Medical University Animals Laboratory (Guangzhou, Guangdong, China). All animals were anesthetized with methoxyfluorane before injection of A549 cells. To establish A549 tumor xenograft model, 2×10^6 A549 cells were suspended in 100 μl PBS and injected via 27-gauge needle into the subcutaneous (s.c.) space of the flank region. Tumors were measured every other day using calipers, and their volumes were calculated by the following formula: $0.5 \times \text{length} \times \text{width}^2$. The animals' body weight was monitored every other day. When tumor volume reached ~100 mm^3, mice were divided into two groups, control group (n = 5) and treatment group (n = 5). Then, taxol in 50 mg/kg was injected intratumorally into growing tumor in treatment group on day 1 and day 19 and saline was injected intratumorally into growing tumor in control group on day 1 and day 19. Mice in blank group (n = 5) had no tumor and treatment.

HISTOLOGICAL ANALYSIS

The organs from all animals were resected, measured and fixed in 4% formaldehyde solution. The tissue slides were processed into paraffin and 5-μm sections were stained with hematoxylin and eosin for histological evaluation.

TRANSMISSION ELECTRON MICROSCOPY

Tumors were fixed by immersion in 2.5% glutaraldehyde in 0.1 M Sorensen buffer, post-fixed in 1% osmium tetroxide, and stained in 3% uranyl acetate. The cells were dehydrated in ethanol and embedded in Epon. Ultra-thin sections were post-stained with uranyl acetate and lead citrate and examined using a Philips CM100 electron microscope at 60 kV. Images were recorded digitally with a Kodak 1.6 Megaplus camera system operated using AMT software (Advanced Microscopy Techniques, Danvers, MA).

STATISTICAL ANALYSIS

Data were presented as means ± SD. Statistical analysis was performed using ANOVA, or student's *t*-test when appropriate. Significance was established when $P < 0.05$. All experiments were performed in a minimum of three times. Survival was analyzed by Kaplan–Meier method, and groups were compared by log-rank analysis.

RESULTS

TAXOL INDUCES PARAPTOSIS-LIKE CELL DEATH IN A549 CELLS IN VITRO

We recently demonstrated that taxol (70 μM) induced paraptosis independent of both protein synthesis and MAPK pathway in ASTC-a-1 cells [Sun et al., 2010]. In A549 cells, CCK-8 assay showed that treatment with different concentrations of taxol for 24 h induced dose-dependent cytotoxicity, and larger than 35 μM of taxol significantly inhibited cell viability (Fig. 1A). In what follows, 70 μM of taxol was adopted in the experiments without indicated concentration. To explore whether taxol induces paraptosis in A549 cells, we used confocal imaging to assess whether taxol induced cytoplasmic vacuolization of cells expressing EGFP, and found that treatment with taxol for 24 h induced significant cytoplasmic vacuolization (Fig. 1B), and the statistical results of cells showing cytoplasmic vacuolization at 0, 3, 6, 9, 12, 18, and 24 h after taxol treatment from at least 300 cells in three independent experiments (Fig. 1C). Taxol induced time-dependent cytoplasmic vacuolization, peaking at around 18 h after taxol treatment (Fig. 1C). These data demonstrated that taxol induced cell death through cytoplasmic vacuolization in vitro.

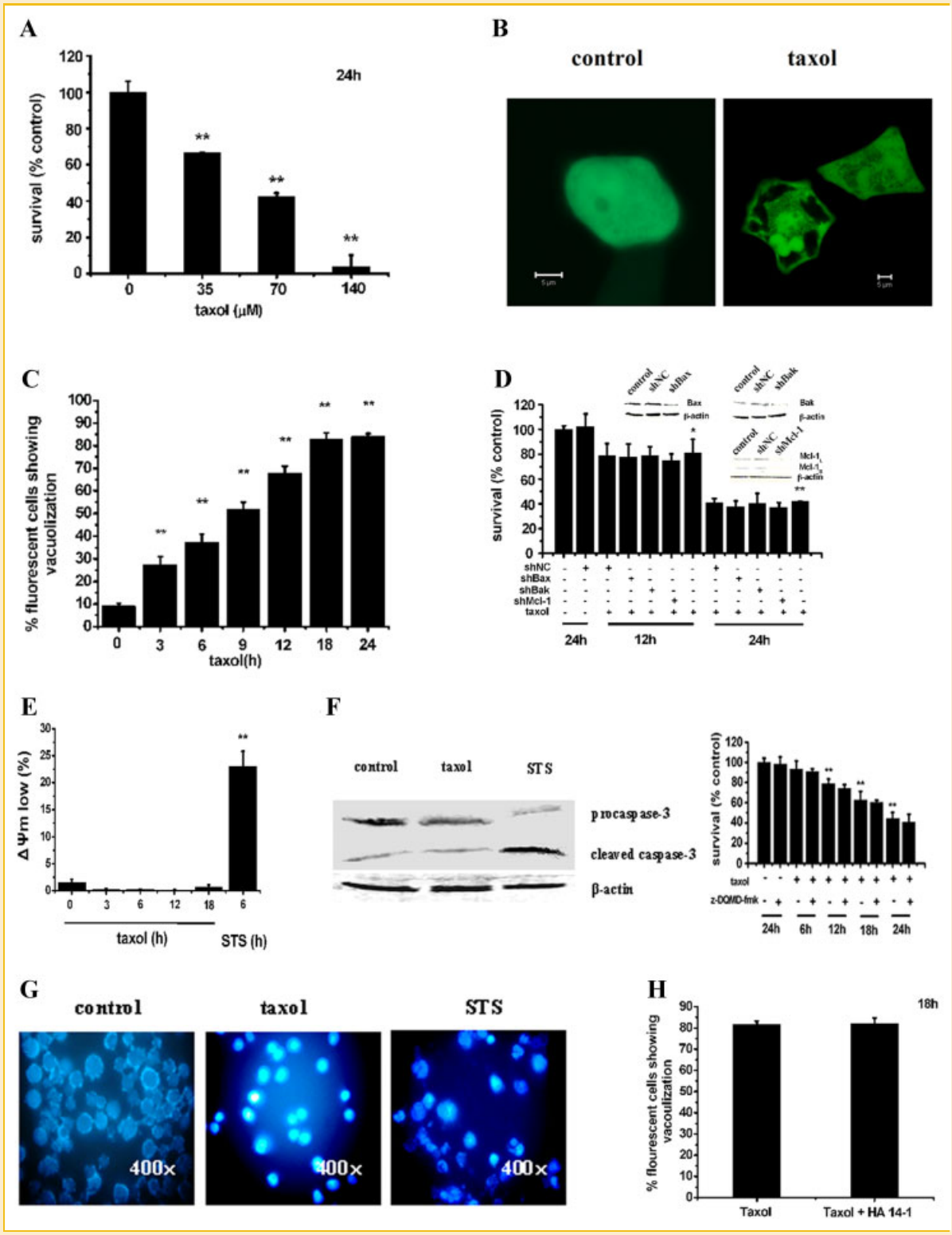

Fig. 1.

Silencing techniques shRNA was used to examine the roles of Bax, Bak, and Mcl-1 during taxol-induced cytotoxicity. shBax, shBak, and shMcl-1 induced significant down-regulation of the expression levels of Bax, Bak, and Mcl-1 (inset figures in Fig. 1D), but did not attenuate taxol-induced cell death (Fig. 1D), suggesting that Bax, Bak, and Mcl-1 did not participate in taxol-induced cell death. FCM was used to analyze the loss of mitochondrial membrane potential ($\Delta\Psi m$) in taxol-treated cells, and the percentage of cells

with low $\Delta\Psi$m were 1.55, 0.3, 0.25, 0.2, and 0.7% after treatment with taxol for 0, 3, 6, 12, and 18 h, respectively (Fig. 1E), implying that taxol did not induce loss of mitochondrial membrane potential. STS (1 μM)-treated cells were used as positive control. In addition, Western blotting analysis demonstrated that taxol did not activate caspase-3, and pretreatment with zDQMD-fmk (10 μM), an inhibitor of caspase-3, also did not prevent taxol-induced cytotoxicity (Fig. 1F), suggesting that caspase-3 was not involved in the taxol-induced cell death. Furthermore, Hoechst 333258 staining showed that taxol only induced nuclear condensation, but did not induced nuclear fragmentation, which was not similar to the STS-treated cells (Fig. 1G).

It has reported that co-expression of Bcl-XL and Bak provokes extensive cytoplasmic vacuolization due to ER swelling [Klee and Pimentel-Muiños, 2005], which is very similar to the taxol-induced cytoplasmic vacuolization. Moreover, our previous report showed that Bcl-XL localized around the taxol-induced swelling ER [Sun et al., 2010]. However, it is unclear whether Bcl-XL participates in the taxol-induced cytoplasmic vacuolization. Here, we assessed the effects of HA14-1 (10 μM), a general inhibitor of Bcl-XL, on taxol-induced cytoplasmic vacuolization. Cells expressing EGFP plasmids were pretreated with HA14-1 for 1 h before taxol treatment. We found that taxol-induced cytoplasmic vacuolization was not inhibited by HA14-1 pretreatment (Fig. 1H), implying that Bcl-XL did not participate in taxol-induced cytoplasmic vacuolization.

Taken together, taxol-induced cell death in a paraptosis-like fashion in A549cells.

ER STRESS DOES NOT PARTICIPATE IN TAXOL-INDUCED CYTOPLASMIC VACUOLIZATION

It is reported that cytoplasmic vacuolization induced by MG132, a proteasome inhibitor, or by inhibition of Hsp 90 and proteasome also involve ER stress [Mimnaugh et al., 2004; Ding et al., 2007]. To determine the relationship between taxol-induced cytoplasmic vacuolization and ER stress, we assessed the role of ATF6, an inducer of ER chaperone proteins, in taxol-induced cytoplasmic vacuolization. Western blotting analysis showed that treatment with taxol for 6 h significantly induced ATF6 cleavage (Fig. 2A) indicative of ER stress. DTT (2 mM)-treated cells were used as positive control.

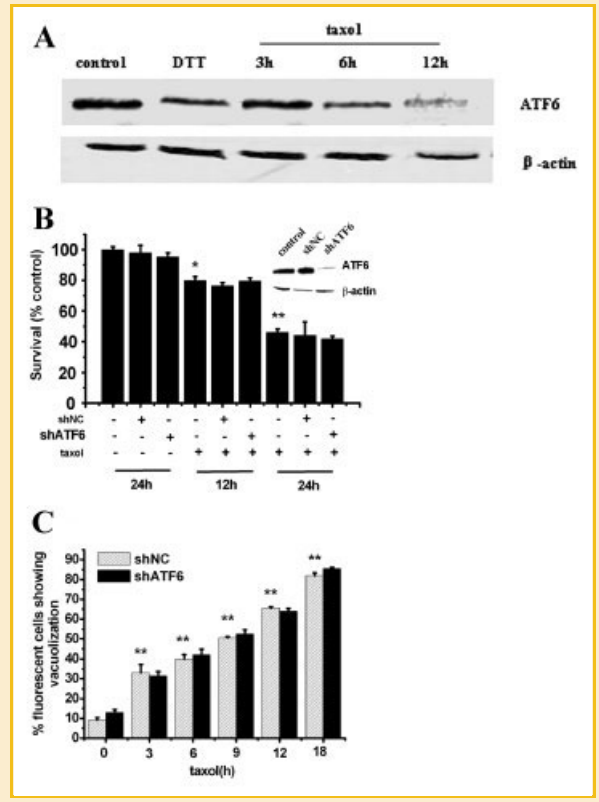

Fig. 2. Taxol-induced ER vacuolization precedes ER-stress. A: Western blotting analysis of taxol-induced cleavage of ATF6. Cells were treated with taxol for 3, 6, and 12 h, and DTT (2 mM, 6 h)-treated cells were used as a positive control. B: Silencing ATF6 did not attenuate taxol-induced cell death by CCK-8 assay. Cells were treated by taxol for 12 or 24 h, respectively. Data are means ± SD (n = 3; ANOVA: $^{**}P < 0.01$, compared with control cells). Western blotting analysis was used to demonstrate the silencing effect of shATF6 plasmids. C: Percentage of vacuolated cells transfected with shNC or shATF6 at 3, 6, 9, 12, and 18 h after taxol treatment. At least 150 cells were scored for each experimental point. Error bars show SDs of percentage obtained by counting at least 10 different fields. $^{**}P < 0.01$, compared with control cells. ATF6, activating transcription factor 6; CCK-8, cell counting kit; DTT, dithiothreitol.

Fig. 1. Taxol induces paraptosis-like cell death in A549 cells. A: Taxol induced dose-dependent reduction of cell viability detected by CCK-8 assay. Cells were seeded into 96-well flat-bottomed microplate and incubated with different concentration of taxol for 24 h. Data are means ± SD (n = 3; ANOVA: $^{**}P < 0.01$, compared with control cells). B: Typical confocal images of cells showing cytoplasmic vacuolization induced by taxol. The cells expressing EGFP were treated without (*control*) or with 70 μM taxol (*taxol*) for 24 h. Scaled bar: 5 μm. C: Percentage of vacuolated cells at 0, 3, 6, 12, 18, or 24 h, respectively, after treatment with taxol. At least 300 cells were scored for each experimental point. Error bars show SDs of percentages obtained by counting at least 10 different fields. $^{**}P < 0.01$, compared with control cells. D: Effects of silencing Bax, Bak, or Mcl-1 on the cytotoxcity of taxol detected by CCK-8 assay. Cells were treated with taxol for 12 or 24 h, respectively. Data are means ± SD (n = 3; ANOVA: $^{**}P < 0.01$, compared with control cells). Western blotting analysis was used to demonstrate the silencing effect of shBax, shBak, and shMcl-1 plasmids. E: Taxol did not induce loss of mitochondrial membrane potential by FCM assay. STS (1 μM)-treated cells were used as a positive control, and cells were treated with taxol for 0, 3, 6, 12, and 18 h, respectively. Data are means ± SD (n = 3; ANOVA: $^{**}P < 0.01$, compared with control cells). F: Caspase-3 did not participate in taxol-induced cell death. *Left*: Western blotting analysis of caspase-3 activation after taxol treatment. Cells were treated with taxol for 24 h, and STS (1 μM)-treated cells were used as a positive control. *Right*: CCK-8 assay of the effect of zDQMD-fmk, an inhibitor of caspase-3, on the taxol-induced cytotoxicity. Cells were treated with taxol for 6, 12, 18, and 24 h in the presence or absence of 10 μM zDQMD-fmk. Data are means ± SD (n = 3; ANOVA: $^{**}P < 0.01$, compared with control cells). G: Fluorescence images of cells stained with Hoechst 333258 at 0 and 24 h after 70 μM taxol treatment. STS (1 μM)-treated cells were used as a positive control. Magnification: 400×. H: Percentage of vacuolated cells expressing EGFP at 24 h after treatment with taxol alone or cotreatment with both taxol and 10 μM HA 14-1. At least 200 cells were scored for each experimental point. Error bars show SDs of percentage obtained by counting at least 15 different fields. $^{**}P < 0.01$, compared with control cells. CCK-8, cell counting kit; DQMD, D(OMe)QMD(OMe); EGFP, enhanced green fluorescent protein; FCM, flow cytometry; STS, staurosporine.

However, silencing ATF6 did not prevent taxol-induced not only cytotoxicity but also cytoplasmic vacuolization (Fig. 2B and C), implying that ER stress was not the upstream event of taxol-induced cytoplasmic vacuolization.

TAXOL-INDUCED CELL DEATH IS NOT SENESCENCE

Senescence was quantified according to morphologic appearance of enlarged, flattened morphology, and vacuolization [O'Callaghan-Sunol et al., 2007], and vacuolization in senescence is irreversible [Frippiat et al., 2001]. To explore whether taxol-induced vacuolization is reversible after weeding out taxol, the cells expressing EGFP plasmids were treated with taxol for 6 h, and then refreshed the culture medium without taxol for another 24 h. We found that the percentage of cells showing vacuolization was about 33% at 6 h after taxol treatment, and did not decrease but increase to 50% without taxol for another 24 h (Fig. 3A), implying that taxol-induced vacuolization is irreversible similar to the senescence.

Another typical marker of senescence in human cells is the senescence-associated β-galactosidase (SA-β-gal) active at pH 6.0, and this activity was shown to correlate with senescence in aging cell cultures in vitro and in vivo [Dimri et al., 1995]. To confirm whether taxol induced cell death in senescence form, H_2O_2 (300 μM)- or taxol-treated cells were stained by Senescence β-Galactosidase Staining Kit, and subsequently imaged using bright-light microscope. Our data showed that the percentage of cells with blue were 65% and 10% for H_2O_2-treated cells, as positive control of senescence [Frippiat et al., 2001], and taxol-treated cells, respectively (Fig. 3B), indicating that H_2O_2 treatment induced senescence, while taxol-induced paraptosis-like cell death was not in senescence fashion.

INTRATUMORAL INJECTION OF TAXOL IN VIVO SUPPRESSES A549 TUMOR WITH ER SWELLING

We established A549 tumor xenograft model to determine whether taxol can exert antitumor effects by inducing ER vacuolization in vivo. Tumors were treated intratumorally both on day 1 and day 19. Therapeutic effects were evaluated by examining tumor growth. As shown in Figure 4B, taxol (50 mg/kg) resulted in 73% tumor growth inhibition (compared to control mice treated with saline) in the xenograft tumor model ($P < 0.05$). Moreover, based on observation of body weight (Fig. 4C), no other host toxicities were observed.

As further validation of the mechanism by which taxol exerts its effects, we assessed the in vivo ER vacuolization analyzed by transmission electron microscopy imaging. Consistent with the in vitro findings, we observed striking cytoplasmic vacuolization from ER (Fig. 4D), and the ER width increased obviously from 0.1 μm (Control) to 0.5 μm (taxol) from at least 200 ER in 15 different cells (Fig. 4E), confirming that taxol inhibited tumor proliferation by inducing ER vacuolization.

IN VIVO ACTIVITY OF TAXOL

To determine whether taxol treatment results in toxicities in vivo, we examined tissue sections of the liver and kidney of tumor-bearing mice by hematoxylin and eosin staining. As shown in Figure 5A, the liver showed normal hepatocytes, and the kidneys showed normal glomeruli, tubules, demonstrating that taxol did not cause any detectable pathologic abnormalities in the mice. To assess

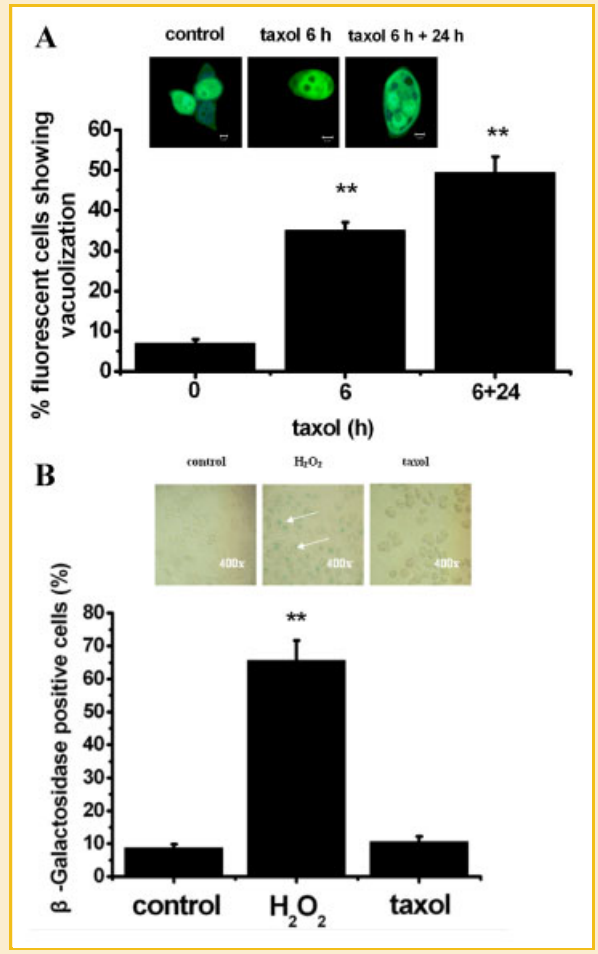

Fig. 3. Taxol-induced cell death is not senescence. A: Percentage of cells showing cytoplasmic vacuolization after exposure of the cells to taxol alone for 6 h (*taxol 6 h*) or to fresh medium for 24 h after taxol treatment for 6 h (*taxol 6 h + 24 h*) analyzed by confocal imaging. At least 300 cells were scored for each experimental point. Data are means ± SD (n = 3; ANOVA: $^{**}P < 0.01$, compared with control cells). Error bars show SDs of percentage obtained by counting at least 10 different fields. $^{**}P < 0.01$, compared with control cells. Scaled bar: 5 μm. B: Percentage of β-gal positive cells determined by counting four random fields under a brightfield microscope. At least 100 cells were recorded from 10 different fields. Magnification: 400x. Data are means ± SD (n = 3; ANOVA: $^{**}P < 0.01$, compared with control cells).

the effect of taxol on the survival time of mice, tumor-bearing mice were divided into two groups (n = 5): taxol- and saline-treated group. The mouse was euthanized when the size of tumor reached 4,000 mm^3 or ulceration. The median survival increased from 39 days in control group to 74 days in taxol-treated group ($P = 0.005$) (Fig. 5B), implying that intratumoral injection of taxol potently prolongs life time without obvious pathologic abnormalities.

DISCUSSIONS

In this investigation, we reveal that taxol is capable of inducing paraptosis-like cell death in A549 cells. In addition, the data that

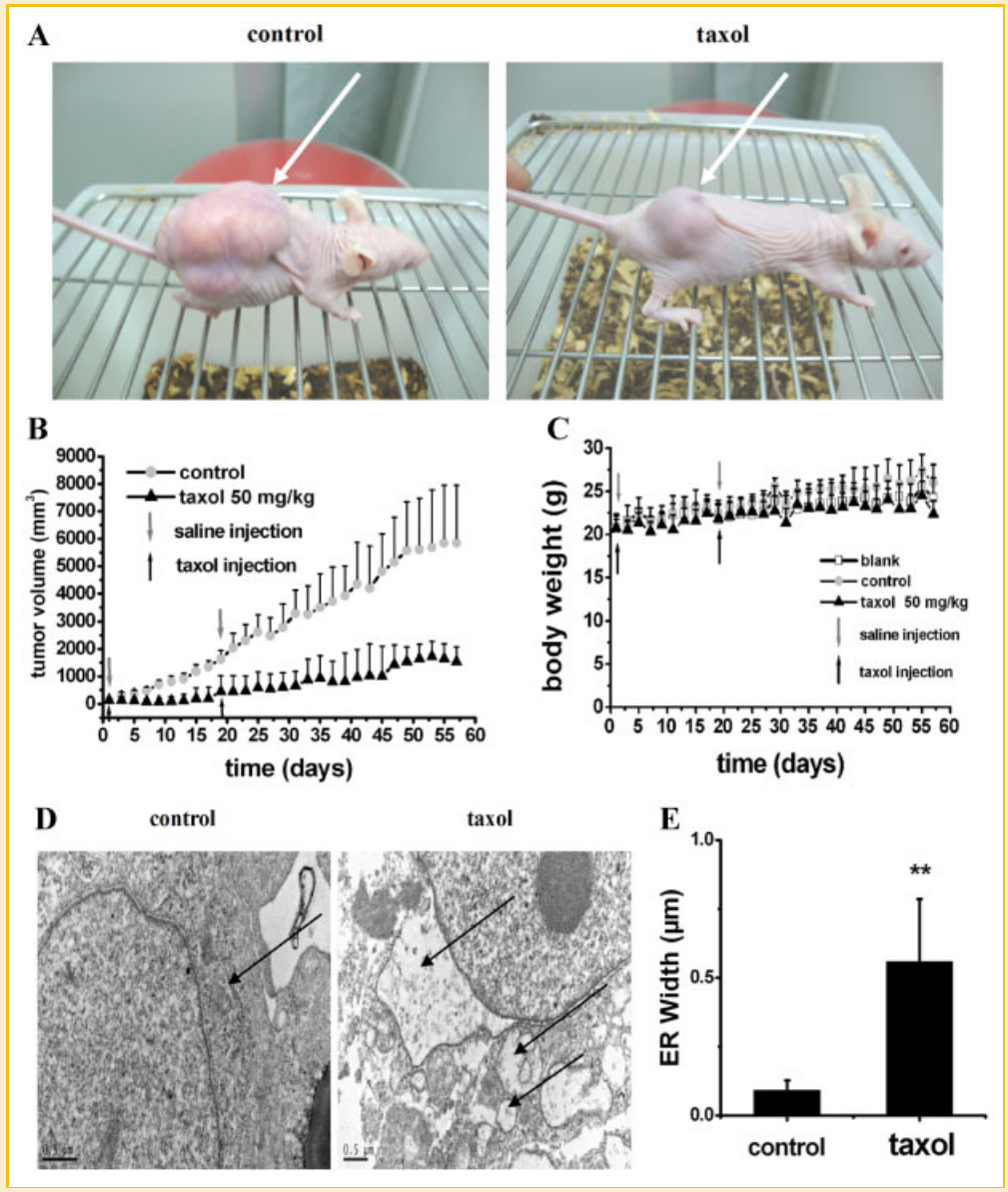

Fig. 4. Intratumoral injection of taxol inhibits tumor growth and induces ER vacuolization in A549 tumor xenograft model. The dose of taxol administered was 50 mg/kg. The mice bearing A549 tumor were treated with saline (*control*) and taxol (*taxol*) intratumorally on day 1 and day 19. A: General appearance of A549 tumors in control group and taxol group. B and C: Inhibition of tumors growth, and the corresponding body weight changes during treatments. D and E: Transmission electron microscopy imaging for control and taxol-treated tumor tissue showing ER (*black arrows*), and the corresponding ER width obtained from at least 200 ER in at least 15 different cells. $^{**}P < 0.01$, compared with control.

taxol-induced cell death with cytoplasmic vacuolization is not senescence further demonstrate our previous notion that taxol induces paraptosis-like cell death [Chen et al., 2008; Sun et al., 2010]. Of the utmost importance, this report firstly demonstrate that intratumoral injection with 50 mg/kg of taxol can remarkably inhibit tumor growth with striking ER vacuolization in vivo without obvious pathologic abnormalities, which may provide a novel potential implication for the forefront of innovative strategies for cancer treatment.

Our observations here further demonstrate our previous finding that taxol induces paraptosis-like cell death [Chen et al., 2008; Sun et al., 2010]. Various forms of cell death, such as oncosis and senescence, have in common that they are executed by cytoplasmic vacuolization [Majno and Joris, 1995; Chang et al., 1999]. Oncosis generally occurs in seconds to minutes at most 1 h and the lysis of cells can be observed in short time, and vacuoles were mainly from mitochondria and smooth ER [Trump et al., 1997; Loo et al., 2007; Cao et al., 2010]. The fact that taxol induces time-dependent cytoplasmic vacuolization, peaking at around 18 h after taxol treatment (Fig. 1C), and the vacuoles is from rough ER (Fig. 4D) demonstrate that taxol-induced cell death is not oncosis. In addition, the cells in senescence also show the characteristics of cytoplasmic vacuolization [Hayflick and Moorhead, 1961; Smith and Pereira-Smith, 1996; Duncan and Reddel, 1997]. However, our data that

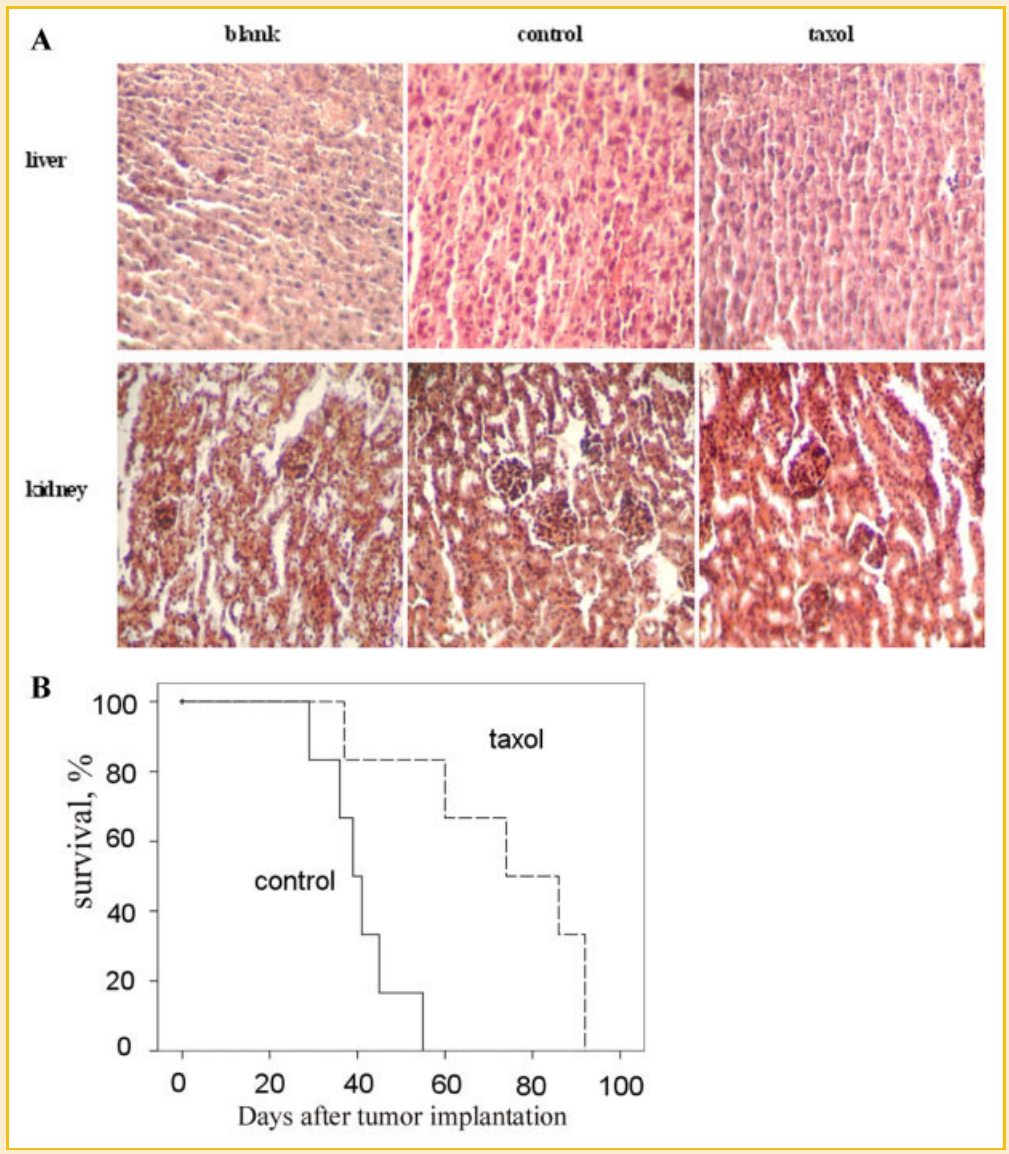

Fig. 5. *In vivo* activity of taxol. A: Microscopic view of the liver and kidney stained by HE (hematoxylin and cosin). The kidneys and livers were harvested from control and taxol-treated mice on day 21. B: Survival was improved in animals treated with taxol by intratumoral injection. $P = 0.005$.

taxol-induced cell death did not show the SA-b-gal positive (Fig. 3B) suggest that taxol-induced cell death is not senescence. In addition, besides lack of caspase-3 activation (Fig. 1F) and DNA fragmentation (Fig. 1G), consistent with our previous report [Chen et al., 2008; Sun et al., 2010], the present study further demonstrated that Bax, Bak, Mcl-1 (Fig. 1D), and Bcl-XL (Fig. 1H) were not involved in the taxol induced paraptosis-like cell death without a significant loss of mitochondrial membrane potential (Fig. 1E), which were the typical biochemical characteristics of paraptosis [Sperandio et al., 2000].

In our previous report, we speculated that taxol-induced cytoplasmic vacuolization derived dominantly from ER may be due to taxol-induced ER stress [Sun et al., 2010]. However, we here found that although taxol induced ER stress (Fig. 2A), silencing ATF6 did not prevent taxol-induced both cytotoxicity and cytoplasmic vacuolization (Fig. 2B and C), indicating that ER stress is not the event mediating the taxol-induced cytoplasmic vacuolization. There are three ER stress receptors, pancreatic ER kinase (PKR)-like ER kinase (PERK), activating transcription factor 6 (ATF6) and inositol-requiring enzyme 1 (IRE1), and the activation of the receptors occurs sequentially, with PERK being the first, rapidly followed by cleavage of ATF6, whereas IRE1 is activated last [Szegezdi et al., 2003]. ATF6 translocates to the Golgi apparatus where it is cleaved into its active form by site-1 and site-2 proteases, and active ATF6 subsequently moves to the nucleus and induces genes with an ER stress response element (ERSE) in their promoter [Schroder and Kaufman, 2005]. Moreover, ATF6 induces ER chaperone proteins such as GRP78, GRP94, and protein disulphide isomerase, which help cells go through ER stress and survive [Szegezdi et al., 2003]. Our data that ATF6 is cleaved at 6 h

(Fig. 2A), but exposure of cells to taxol for 3 h induces significant vacuolization (Fig. 1C) suggests that taxol-induced ER vacuolization precedes ER stress. In addition, the fact that silencing ATF6 by shATF6 does not prevent taxol-induced cell death and cytoplasmic vacuolization (Fig. 2B and C) further demonstrate that ATF6 does not participate in taxol-induced paraptosis-like cell death. Therefore, it is reasonable to speculate that taxol-induced cytoplasmic vacuolization is not from ER stress.

Our observations that taxol (70 μM) induces a rapid ER vacuolization and paraptosis-like cell death without apoptotic characteristics, such as apoptotic body, Bax/Bak activation, caspases activation, DNA fragmentation, and the involvement of Bcl-XL and Mcl-1 (Fig. 1), suggest that ER but not mitochondria plays an important role in taxol-induced cell death. Liao et al. [2008] demonstrated that taxol (100 μM) induced ER stress after 1–3 h of treatment similar with our observation (Fig. 2A), whereas the mitochondria-related apoptosis events, such as caspase activation and cytochrome c translocation, occurs at 9–12 h after taxol treatment in U937 cells [Liao et al., 2008]. In fact, our previous report showed that low concentration of taxol (35 nM) induced cell death dominantly in apoptotic fashion in which significant ER vacuolization was observed, but which mainly occurred at 48 h after taxol treatment [Guo et al., 2010; Sun et al., 2010]. Moreover, we here found that taxol-induced ER vacuolization precedes ER stress (Fig. 2). Therefore, we speculate that high concentration of taxol induces a rapid ER stress and ER vacuolization within 6 h, which mediates paraptosis-like cell death in mitochondria-independent pathway before triggering apoptotic signaling pathway. It is also possible that high concentration of taxol directly damages mitochondria and hinders the process of mitochondrial apoptosis signaling pathways, which is supported by our previous data that high concentration of taxol also induces mitochondrial swelling [Chen et al., 2008; Sun et al., 2010].

Our in vivo data that intratumoral injection of taxol suppress tumor growth with ER vacuolization (Fig. 4) further provide an important cue for seeking a new target of the action of drug for cancer therapy to overcome the drug-resistance that is the main difficulties and obstacles for all specialists [Fields and Runowicz, 2003; Crown et al., 2004; Hocsak et al., 2010]. NSCLC is the most lethal malignant cancer disease worldwide [Pallis et al., 2009]. The acquired drug resistance of tumor cells and cumulative side effects of the cytotoxic agent present serious clinical obstacles [Szanto et al., 2009; Rabah, 2010]. Resistance and evasion of apoptosis are critical factors that contribute to carcinogenesis and drug resistance [Hu and Kavanagh, 2003; Isoldi et al., 2005]. Intratumoral chemotherapy focuses high drug concentrations in solid tumors and limits total body exposure to the cytotoxic agent, resulting in increased dose-related killing of tumor cells at reduced, or at least equivalent, systemic toxic effects [Jackson et al., 2000]. Yoo et al. [2005] found that intratumoral injection of taxol (15 mg/kg) inhibited growth of tumor by inducing apoptosis. Here, we found that intratumoral injection with 50 mg/kg of taxol not only prolonged life span without obvious side effect (Fig. 5) but also induced a significant ER vacuolization in vivo (Fig. 4D and E). In combination with the result that taxol induces mitochondria-independent paraptosis-like cell death in vitro, it is reasonable to use local intratumoral injection of high concentration of taxol to kill the apoptosis-resistance cancer.

In summary, high concentration of taxol induces paraptosis-like cell death via an ER vacuolization-mediated pathway independent of mitochondria and ER stress, in which Bax, Bak, Mcl-1, Bcl-XL, and caspase-3 are not involved. Moreover, intratumoral injection of high concentration of taxol suppresses tumor proliferation and induces ER vacuolization in vivo. Although the study was performed in mice, we believe that the intratumoral injection of taxol may offer a potentially effective therapy for patients with drug-resistant cancer and for some patients with localized tumors who are not candidates for radical treatment.

REFERENCES

Al-Ghananeem AM, Malkawi AH, Muammer YM, Balko JM, Black EP, Mourad W, Romond E. 2009. Intratumoral delivery of paclitaxel in solid tumor from biodegradable hyaluronan nanoparticle formulations. AAPS Pharm Sci Tech 10:410–417.

Cao X, Zhang Y, Zou L, Xiao H, Chu Y, Chu X. 2010. Persistent oxygen-glucose deprivation induces astrocytic death through two different pathways and calpain-mediated proteolysis of cytoskeletal proteins during astrocytic oncosis. Neurosci Lett 479:118–122.

Celikoglu F, Celikoglu SI, Goldberg EP. 2008. Bronchoscopic intratumoral chemotherapy of lung cancer. Lung Cancer 61:1–12.

Chang BD, Broude EV, Dokmanovic M, Zhu H, Ruth A, Xuan Y, Kandel ES, Lausch E, Christov K, Roninson IB. 1999. A senescence-like phenotype distinguishes tumor cells that undergo terminal proliferation arrest after exposure to anticancer agents. Cancer Res 59:3761–3767.

Chen TS, Wang XP, Sun L, Wang LX, Xing D, Mok M. 2008. Taxol induces caspase-independent cytoplasmic vacuolization and cell death through endoplasmic reticulum (ER) swelling in ASTC-a-1cells. Cancer Lett 270: 164–172.

Crown J, O'Leary M, Ooi WS. 2004. Docetaxel and paclitaxel in the treatment of breast cancer: A review of clinical experience. Oncologist 9(Suppl 2): 24–32.

Duncan EL, Reddel RR. 1997. Genetic changes associated with immortalization. Biochemistry 62:1263–1274.

Dimri GP, Lee X, Basile G, Acosta M, Scott G, Roskelley C, Medrano EE, Linskens M, Rubelj I, Pereira-Smith O, Peacocke M, Campisi J. 1995. A biomarker that identifies senescent human cells in culture and in aging skin *in vivo*. Proc Natl Acad Sci USA 92:9363–9367.

Ding WX, Ni HM, Yin XM. 2007. Absence of Bax switched MG132-induced apoptosis to non-apoptotic cell death that could be suppressed by transcriptional or translational inhibition. Apoptosis 12:2233–2244.

Fields AL, Runowicz CD. 2003. Current therapies in ovarian cancer. Cancer Invest 21:148–156.

Frippiat C, Chen QM, Zdanov S, Magalhaes JP, Remacle J, Toussaint O. 2001. Subcytotoxic H_2O_2 stress triggers a release of transforming growth factor-β1, which induces biomarkers of cellular senescence of human diploid fibroblasts. J Biol Chem 276:2531–2537.

Guo WJ, Chen TS, Wang XP, Chen R. 2010. Taxol induces concentration-dependent apoptotic and paraptosis-like cell death in human lung adenocarcinoma (ASTC-a-1) cells. J X-ray Sci Technol 18:293–308.

Hayflick L, Moorhead PS. 1961. The serial cultivation of human diploid cell strains. Exp Cell Res 37:585–621.

Hocsak E, Racz B, Szabo A, Pozsgai E, Szigeti A, Szigeti E, Gallyas F Jr, Sumegi B, Javor S, Bellyei S. 2010. TIP47 confers resistance to taxol-induced cell death by preventing the nuclear translocation of AIF and Endonuclease G. Eur J Cell Biol 89:853–861.

Horwitz SB, Cohen D, Rao S, Ringel I, Shen HJ, Yang CP. 1993. Taxol: Mechanisms of action and resistance. J Natl Cancer Inst Monogr 15:55–61.

Hu W, Kavanagh JJ. 2003. Anticancer therapy targeting the apoptotic pathway. Lancet Oncol 4:721–729.

Ishibashi M, Nakayama K, Yeasmin S, Katagiri A, Iida K, Nakayama N, Fukumoto M, Miyazaki K. 2008. A BTB/POZ gene, NAC-1, a tumor recurrence-associated gene, as a potential target for taxol resistance in ovarian cancer. Clin Cancer Res 14:3149–3155.

Isoldi MC, Visconti MA, Castrucci AM. 2005. Anti-cancer drugs: Molecular mechanisms of action. Mini Rev Med Chem 5:685–695.

Jackson JK, Gleave ME, Yago V, Beraldi E, Hunter WL, Burt HM. 2000. The suppression of human prostate tumor growth in mice by the intratumoral injection of a slow-release polymeric paste formulation of paclitaxel. Cancer Res 60:4146–4151.

Klee M, Pimentel-Muiños FX. 2005. Bcl-XL specifically activates Bak to induce swelling and restructuring of the endoplasmic reticulum. J Cell Biol 168:723–734.

Li YL, Xing D, Chen Q. 2009. Dynamic monitoring of apoptosis in chemotherapies with multiple fluorescence reporters. Mol Imaging Biol 11:213–222.

Liao PC, Tan SK, Lieu CH, Jung HK. 2008. Involvement of endoplasmic reticulum in paclitaxel-induced apoptosis. J Cell Biochem 104:1509–1523.

Loo D, Pryer N, Young P, Liang T, Coberly S, King KL, Kang K, Roberts P, Tsao M, Xu X, Potts B, Mather JP. 2007. The glycotope-specific RAV12 monoclonal antibody induces oncosis *in vitro* and has antitumor activity against gastrointestinal adenocarcinoma tumor xenografts *in vivo*. Mol Cancer Ther 6:856–865.

Lu Y, Chen T, Wang XP, Qu JL, Chen M. 2010. The JNK inhibitor SP600125 enhances dihydroartemisinin-induced apoptosis by accelerating Bax translocation into mitochondria in human lung adenocarcinoma cells. FEBS Lett 584:4019–4026.

Mailloux A, Grenet K, Bruneel A, Bénéteau-Burnat B, Vaubourdolle M, Baudin B. 2001. Anticancer drugs induce necrosis of human endothelial cells involving both oncosis and apoptosis. Eur J Cell Biol 80:442–449.

Majno G, Joris I. 1995. Apoptosis, oncosis, and necrosis: An overview of cell death. Am J Pathol 146:3–15.

Mimnaugh EG, Xu W, Vos M, Yuan X, Isaacs JS, Bisht KS, Gius D, Neckers L. 2004. Simultaneous inhibition of hsp 90 and the proteasome promotes protein ubiquitination, causes endoplasmic reticulum-derived cytosolic vacuolization, and enhances antitumor activity. Mol Cancer Ther 3:551–566.

Monzó M, Rosell R, Sánchez JJ, Lee JS, O'Brate A, Gonzalez-Larriba JL, Alberola V, Lorenzo JC, Nunez L, Ro JY, Martin C. 1999. Paclitaxel resistance in non–small-cell lung cancer associated with β-tubulin gene mutations. J Clin Oncol 17:1786–1793.

O'Callaghan-Sunol C, Gabai VL, Sherman MY. 2007. Hsp27 modulates p53 signaling and suppresses cellular senescence. Cancer Res 67:11779–11788.

Pallis AG, Serfass L, Dziadziuszko R, van Meerbeeck JP, Fennell D, Lacombe D, Welch J, Gridelli C. 2009. Targeted therapies in the treatment of advanced/metastatic NSCLC. Eur J Cancer 45:2473–2487.

Pushkarev VM, Starenki DV, Saenko VA, Pushkarev VV, Kovzun OI, Tronko MD, Popadiuk ID, Yamashita S. 2008. Differential effects of low and high doses of taxol in anaplastic thyroid cancer cells: Possible implication of the Pin1 prolylisomerase. Exp Oncol 30:190–194.

Rabah SO. 2010. Acute Taxol nephrotoxicity: Histological and ultrastructural studies of mice kidney parenchyma. Saudi Med J 17:105–114.

Schroder M, Kaufman RJ. 2005. The mammalian unfolded protein response. Annu Rev Biochem 74:739–789.

Shikanov A, Shikanov S, Vaisman B, Golenser J, Domb AJ. 2008. Paclitaxel tumor biodistribution and efficacy after intratumoral injection of a biodegradable extended release implant. Int J Pharm 358:114–120.

Shikanov S, Shikanov A, Gofrit O, Nyska A, Corn B, Domb AJ. 2009. Intratumoral delivery of Paclitaxel for treatment of orthotopic prostate cancer. J Pharma Sci 98:1005–1014.

Smith JR, Pereira-Smith OM. 1996. Replicative senescence: Implications for *in vivo* aging and tumor suppression. Science 273:63–67.

Sperandio S, deBelle I, Bredesen DE. 2000. An alternative, nonapoptotic form of programmed cell death. Proc Natl Acad Sci USA 97:14376–14381.

Stepien A, Grzanka A, Grzanka D, Szczepanski MA, Helmin-Basa A, Gackowska L. 2010. Taxol-induced polyploidy and cell death in CHO AA8cells. Acta Histochem 112:62–71.

Sun QR, Chen TS, Wang XP, Xun BW. 2010. Taxol induces paraptosis independent of both protein synthesis and MAPK Pathway. J Cell Physiol 222:421–432.

Szanto A, Hellebrand EE, Bognar Z, Tucsek Z, Szabo A, Gallyas F, Jr, Sumegi B, Varbiro G. 2009. PARP-1 inhibition-induced activation of PI-3-kinase-Akt pathway promotes resistance to taxol. Biochem Pharmacol 77:1348–1357.

Szegezdi E, Fitzgerald U, Samali A. 2003. Caspase-12 and ER-stress-mediated apoptosis: The story so far. Ann NY Acad Sci 1010:186–194.

Torres K, Horwitz SB. 1998. Mechanisms of taxol-induced cell death are concentration dependent. Cancer Res 58:3620–3626.

Trump BE, Berezesky IK, Chang SH, Phelps PC. 1997. The pathways of cell death: Oncosis, apoptosis, and necrosis. Toxicol Pathol 24:82–88.

Yeung TK, Germond C, Chen XM, Wang ZX. 1999. The mode of action of Taxol: Apoptosis at low concentration and necrosis at high concentration. Biochem Biophys Res Commun 263:398–404.

Yoo GH, Subramanian G, Boinpally RR. 2005. An *in vivo* evaluation of docetaxel delivered intratumorally in head and neck squamous cell carcinoma. Arch Otolaryngol Head Neck Surg 131:418–429.

Yu YL, Su KJ, Chen CJ, Wei CW, Lin CJ, Yiang GT, Lin SZ, Harn HJ, Chen YLS. 2012. Synergistic anti-tumor activity of isochaihulactone and paclitaxel on human lung cancer cells. J Cell Physiol 227:213–222.

Zaman GJ, Flens MJ, van Leusden MR, de Haas M, Mulder HS, Lankelma J, Pinedo HM, Scheper RJ, Baas F, Broxterman HJ. 1994. The human multidrug resistance-associated protein MRP is a plasma membrane drug-efflux pump. Proc Natl Acad Sci USA 91:8822–8826.